DESIGN AND IMPLEMENTATION OF A NOVEL EMBEDDED READOUT ELECTRONICS FOR EXISTING PORTABLE RADIATION INSTRUMENTS

[1]Puja Singh, [2]Ankit

[1]M. Tech. Scholar, [2]Assistant Professor
Electronics & Communication Engineering
CBS Group of Institutions

Abstract*: In the present work, a novel scheme for implementing the GM tube read-out functions is designed, in order to overcome the drawbacks of microprocessor-based designs. This scheme integrates the implementation of the signal processing, HV biasing, data processing and user interface functions onto a single-chip mixed-signal PSoC platform. Pulse count rates from GM tubes exposed to gamma photons are influenced by both exposure rate and gamma energy. This is because a GM tube's inherent detection effectiveness varies with gamma energy. Only an energy adjusted GM tube may be used in the current work on GM counter embedded readout. An energy compensated GM tube is coated with lead and/or tin. This metal coating is used to empirically match the efficiency vs energy curve of a particular tube. This empirical adjustment may be enhanced in situations when the gamma energies in the application of concern are known a priori. Once the survey meter sensitivity versus energy data is obtained, it may be used as a search up table in the firmware. Those correction factors may be incorporated in the firmware's engineering conversion codes. Battery monitoring and testing may be added. Composite dead layers in the unit cell may enhance neutron detector optimization calculations. In Monte Carlo simulations, sophisticated semiconductor detectors such as neutron converter coated avalanche photodiodes with statistically variable multiplication factors may replace basic PIN diode-based devices. The firmware for the alpha spectrometer may be enhanced with isotope identification, user controlled ramping rate, long term stability monitoring, and battery monitoring. More sophisticated reset switch control waveforms and ultra-low charge injection switches may be used to minimize residual errors in pulse height measurement and improve resolution. This study conduct research that has been accomplished in two important aspects of small radiation instruments, in particular, the execution of readout electronics using a novel reconfigurable mixed signal hardware platform, as well as the design and optimization of detectors.

***Keywords*: Portable Radiation Instruments, GM Tube's, Monte Carlo Simulations, PIN Diode-Based Devices**

I. INTRODUCTION

Radioactive materials, radioactive sources, and radiation sources are ubiquitous; they are used in practically all sectors, made of different radionuclides, emit different types of ionizing radiation (gamma rays, alpha and beta particles, neutrons), and are characterized by their activity (number of disintegrations per second). Gamma radiation survey forms the basis of various operational aspects of nuclear industry such as mineral exploration, routine monitoring of activity in and around nuclear facilities, risk assessment during nuclear emergencies etc. "This application demands portable instruments which aid health physics workers in measuring and recording the radiation dose rates at various locations in the field." Over the years, numerous portable instrument designs for gamma survey have been developed. Some of the detectors used in commercially available portable systems include, ion chambers, Geiger- Mueller (GM) tubes and scintillation-based detectors like NaI, CsI, LaBr3 etc. coupled with photo-detectors. Although many types of detectors are available, the detector that finds the most widespread use is the GM tube. This is due to its simple construction and large signal output which aids in implementing cost effective designs. The large signals in the GM tube are the result of a gas avalanche phenomenon known as Geiger discharge which occurs at high voltages (~500V) in a gas filled tube. The avalanche is started by a secondary electron which originally is generated by a gamma interaction either in the solid wall or the gaseous interior of the detector. This original interaction of gamma radiation is by photo-electric absorption, Compton scattering or pair production, which results in transfer of a major portion of gamma energy to the electron in a single interaction. The presence of large signals (> 1V) eliminates the need for precision amplification in the front-end while designing counting and read-out systems. However, the requirements for a stable HV bias, data processing and user interfaces slightly increase the complexity in this system design.

RISKS AND BENEFITS

We all confront dangers in our daily lives. It is difficult to eradicate all of them, but they may be reduced. For example, the usage of coal, oil, and nuclear energy for power generation is linked to some level of health risk, however little. In general, society accepts the risk in exchange for the corresponding advantages. Anyone who is exposed to carcinogenic chemicals runs the risk of developing cancer. In the nuclear sector, every effort is taken to keep such hazards as low as is practically possible.
Radiation protection sets examples for other safety disciplines in two unique respects:

- First, there is the assumption that any increased level of radiation above natural background will carry some risk of harm to health.

- Second, it aims to protect future generations from activities conducted today.

Radiation and nuclear technology have had enormous societal advantages in medical, industry, agriculture, energy, and other scientific and industrial disciplines. In terms of human lives saved, the advantages of medical diagnosis and treatment are significant. Radiation therapy is an important part of the treatment of some cancers. Nuclear medicine is used to treat three out of every four patients in hospitals in developed nations. Similar positive effects may be shown in other disciplines.

There are dangers involved with every human action and habit. Radiation should be regarded in the light of the fact that the advantage it provides to humanity is less hazardous than that provided by many other agents.

GEIGER MUELLER COUNTERS

The GM counter is a basic particle detector that is commonly employed in the detection of nuclear occurrences (Knoll, 2009), and it operates and counts nuclear occurrences with a controlled 500 V bias. The practical collection of data using a GM tube for the purpose of radiation measurement necessitates the use of a signal conditioning circuit, a pulse discriminator, and a digital counter. The sequence of functions in a generic GM counter readout system is described in this study, followed by their implementation on a single chip mixed signal platform.

The following are the sequential functional requirements of GM counter for radiation applications:

- acquisition of raw analogue pulses from GM-tube
- generation of high voltage and biasing the GM tube
- display the counts per second or the dose information.
- counting the logic pulses with time gating
- conditioning the raw pulses to form logic pulses
-

II. PSOC EMBEDDED DESIGN

High resolution alpha spectroscopy is increasingly playing a major role in many radiation measurement applications which include environmental characterization for radiation protection, nuclear fuel cycle, nuclear safeguards and study of geochemical processes. These applications involve the identification of various alpha emitting nuclides and their isotopes present in a sample. The precise location of energy peaks in the spectrum and the determination of the isotopic ratios enable nuclide identification. Hence, the accuracy of the measurements in these applications depends greatly on the quality of the energy spectrum obtained, which is determined largely by the noise performance of the detector and the front-end electronics.

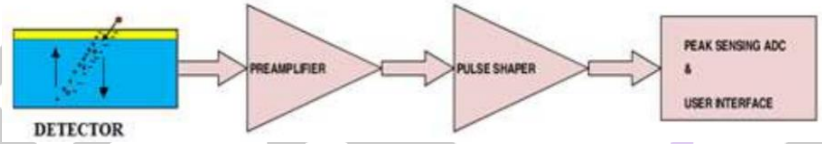

Fig. 1: General alpha spectroscopy system block diagram showing the detector, preamplifier, the pulse shaping filter and the peak sensing circuits

A general alpha spectroscopy system consists of a detector at the first stage, where particles interact and deposit their energy to generate charge pairs. This is followed by a pre-amplifier and pulse shaper at the front-end, using which energy information is mapped to the amplitude of a voltage pulse (figure 1). This chapter describes the design, implementation and performance of an alpha spectrometer in which, a spectral resolution suitable for field measurements is obtained using PIN diode-based detection. Notwithstanding, it provides additional cost benefits by completely eliminating the pulse shaper stage that is mandatorily used in conventional systems for noise elimination and pulse pile-up prevention. This is achieved by utilizing a novel Embedded Pulsed Resistive Reset (EPRR)technique implemented at the pre-amplifier stage, thereby reducing the total number of high-cost analog components. This spectrometer uses a PSoC (Cypress Semiconductor) mixed signal microcontroller platform for both the digitization and embedded reset function. The system design is based on virtual instrumentation and hence, the mixed signal microcontroller platform also performs the data communication with a PC based GUI developed using LabVIEW. The system level description of the spectrometer is given in the next section. The subsequent sections in this chapter describe in detail, the design and implementation of the frontend, its associated EPRR function and the integration of EPRR with the user interface of the alpha spectrometer. The final section depicts the spectrum obtained from the above topology and the results of the same are discussed.

SYSTEM LEVEL MODULAR DESIGN

The PC with GUI, the mixed signal embedded platform, the front-end comprising a pre-amplifier, a reset device, a HV bias block and the dominant noise sources are shown in Figure 2 shows the system level modular design scheme of the spectrometer which consists of three main blocks. "The first is the front-end consisting of the detector (D1), pre-amplifier, HV generator for detector bias and solid-state analog switch as reset device." The second block is a mixed signal embedded platform which acts as the interface between the PC and the front-end. It performs various functions like pulse height digitization, pile-up detection and detector bias regulation. The third block is a virtual instrument GUI that provides a console to the user for spectrum viewing and spectrometer control.

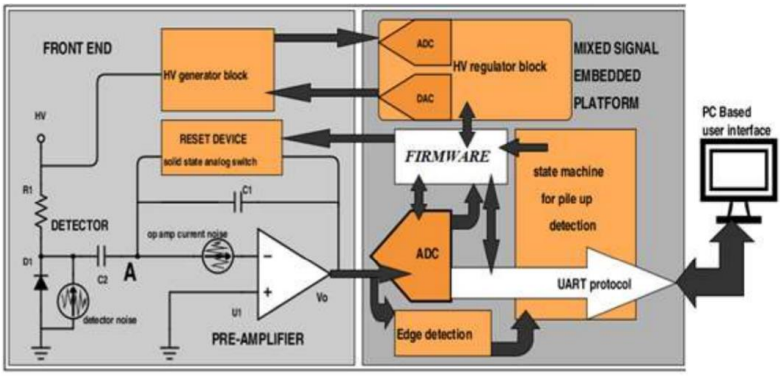

Fig. 2: Block diagram of embedded pulsed reset alpha spectrometer.

FRONT-END DESIGN

The front-end design consists of various sub-component modules like, the detector, its mount, the HV biasing network and the pre-amplifier. The pre-amplifier design mainly involves the selection of COTS components like the Op-Amp to match the detector characteristics and the reset device.

The detector biases

The energy range of alpha particles from naturally occurring sources is between 3 MeV and 7 MeV. The alpha energy deposited in the depletion region of the planar PIN diode alone contributes to the external detector signal. Hence, it should be ensured that the width of the depletion region is always equal to or greater than the range of the highest energy alpha particles (i.e., 7 MeV alpha particles) impinging on the detector. The width of the depletion layer varies with respect to the detector reverse bias and its value is estimated from the detector capacitance measurement using the relation

$$C_d = \epsilon A/d$$

where, Cd is the detector capacitance in Farads (F), is the dielectric constant of silicon material (F/m), A is the area of the diode (100 mm2) and d, the depletion width (m). The variation of depletion width with respect to the reverse bias for the M/s BEL PIN diode used in this work measured experimentally using an LCR meter (M/s Agilent E4980A) at 1 kHz is shown in figure 3. It is estimated from the capacitance values in the figure that for an unbiased diode (0 V reverse bias), the depletion width is typically ~1 µm and is very less compared to 45 µm, which is the approximate range of 7 MeV alpha particles in silicon.

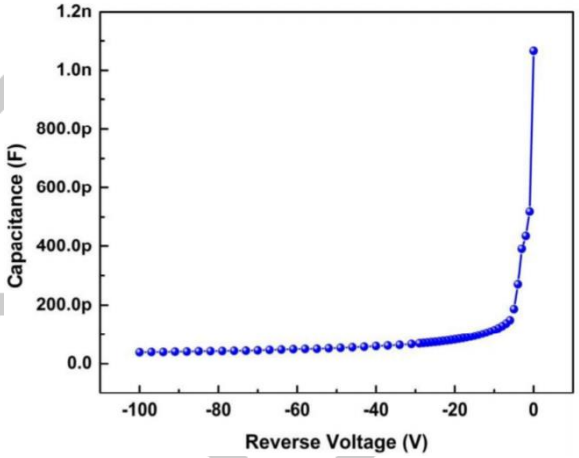

Fig. 3: C-V characteristics of the M/S BEL PIN diode

Detector and its mount

The detector is a planar PIN diode which has a heavily doped shallow p+ and n+ regions on the top and bottom surfaces respectively of a high resistivity n-substrate (a nearly intrinsic- region), originally a part of a silicon wafer (figure 4). The bottom n+ layer provides a good ohmic contact between the n-substrate and an additional aluminum metal layer used for biasing the p+ n junction. Radiation interacts in the depletion region formed in the substrate by reverse biasing the p+ n (intrinsic region) junction to produce electron hole pairs. The electric field present in the depletion region sweeps the electrons towards the n+ region and holes towards the p+ region producing a momentary current pulse in an external circuit which is integrated using a charge sensitive pre-amplifier for generating a charge signal. The most important characteristics used while choosing a detector is its shot noise, which arises out of the leakage current through the reverse biased junction.

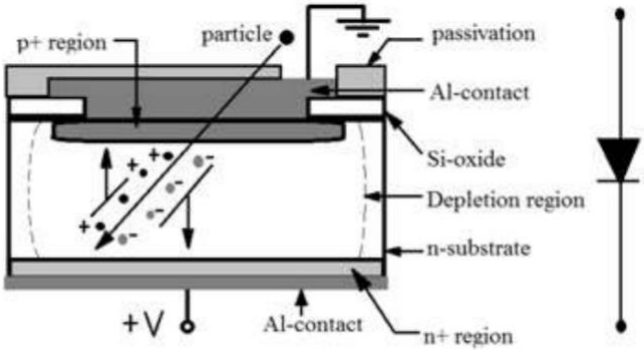

Fig. 4: Structure of Important parts of a planar PIN diode

The spectral density of the shot noise current i_{nd} in terms of the reverse leakage current i_d is given by.

$$i_{nd}^2 = 2ei_d$$

where, e is the charge on an electron. Since the shot noise is directly proportional to the square root of the reverse leakage current, a device with low leakage current is a good choice. The present design uses a commercial 100 mm2 PIN diode (M/s BEL, India) (figure 5 inset), which is made from high resistivity (3.3 K ohm-cm) silicon substrate and has a very low reverse leakage current of 25 nA (design value 10 nA) measured at a voltage of 100 V under reverse biased condition and hence a negligible shot noise level.

Fig. 5: The vacuum chamber used in this work and the PIN diode (inset)

The operation of PIN diode for alpha detection warrants two experimental conditions, namely, experiment should be conducted in dark environment and under vacuum. The sensitivity of the PIN diode surface for ambient light and the energy straggling of alpha particles in air necessitates these conditions. A small vacuum chamber (8.5 x 5 x 7 cm) is made which can support a vacuum of 20 torr (~0.002 MPa), while providing a dark ambience for the diode operation (figure 5).

The preamplifier designs

Owing to the recent availability of low cost, high performance Op-Amps, the efforts on front-end design for portable radiation measurement systems is increasingly being centered around the choice of the best COTS functional blocks. COTS amplifiers have hitherto been employed in pre-amplifier designs for CdTe detector (figure 6 (a)) to obtain high resolution gamma spectroscopy and considerable cost reduction. The capacitance and leakage current characteristics of Si PIN diodes are comparable to CdTe detectors (~100pF for a 21.5 x 21.5 x 0.5mm area CdTe detector). Hence, in this work, an existing pre-amplifier design for CdTe detector has been adopted with requisite modifications for alpha detection using Si PIN diodes. COTS Op-Amp based circuits eliminate the dependence on expensive ASIC or discrete component-based hybrid circuits, which additionally involve substantial circuit design time and complexity in its optimization.

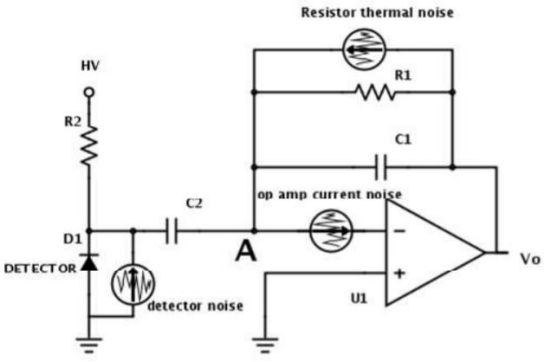

(a) The pre-amplifier configuration with the dominant noise sources

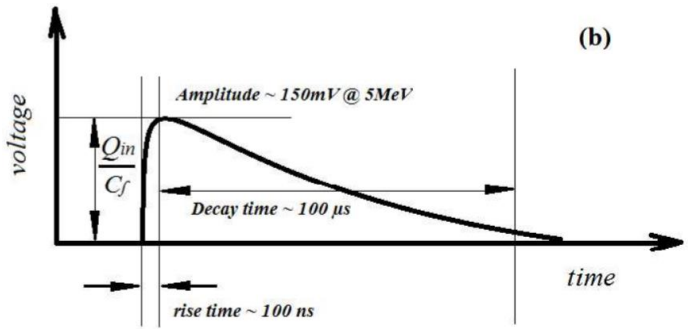

(b) a typical tail pulse output with the resistive reset scheme

Fig. 6: Output of Pre-Amplifier Stage Designed Configuration

The configuration of the pre-amplifier stage designed in this work is a charge sensitive one in which, the output is a voltage tail-pulse signal as shown in figure 6 (b). The step height of the tail-pulse corresponds to the charge generated by an alpha particle in the sensitive region of the detector. The charge sensitivity or the charge gain which is the pulse height voltage per unit charge generated is given by

$$Gain = \frac{1}{C_f}$$

In this design, a feedback capacitor (Cf) value of 1pF is chosen which corresponds to a charge sensitivity of 1V/pC. It is to be pointed out that the capacitance and leakage current characteristics of the input FET had been a prime consideration for the choice of Op-Amp. The charge sensitive pre-amplifier design is matched to the detector using two main detector characteristics namely, Cd and id based on the data obtained from the C-V characteristics shown in figure 3 and the measured reverse leakage current at 100 V. This has been experimentally verified in the gamma spectroscopy application for which it was originally designed. The approach employed for CdTe detectors has been adopted in this present work.

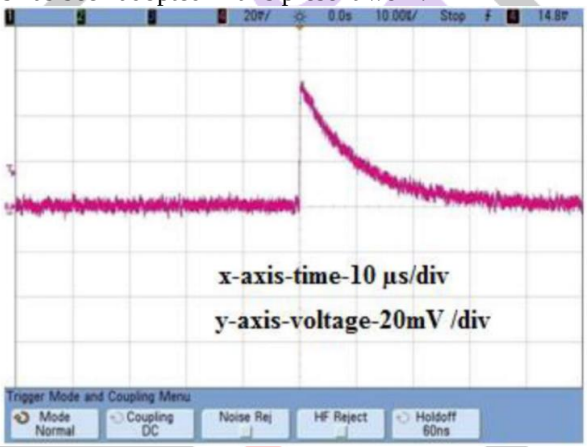

Fig. 7: Preamplifier output with standard resistive reset scheme with a feedback resistor of 10MΩ

The pulse decays to ground level within 30 µs

The output pulse obtained from the pre-amplifier for a 5486 KeV alpha particle from an Am-241 source is shown in the figure 3.7 above. This design uses the commercially available OPA 656 Op-Amp from Texas instruments owing to its salient design capabilities. Its features comprise a 500 MHz wide stable unity gain bandwidth, a FET input stage enabling very low input bias current of 2pA, a very high input impedance and an ultra-low input voltage noise density of 7nV/√Hz. The features make it the best choice for an ultra-low noise charge sensitive pre-amplifier for alpha spectroscopy. In a standard pre-amplifier design, the charge accumulated on C1 is discharged through a parallel resistor R1. This prevents pile-up of pulses from radiation events closely spaced in time, thereby reducing errors in output pulse height measurement.

R1 values in the range of 10MΩ to 100 MΩ are commonly used for moderately quick discharge (~50 µs). Such low resistance values are ideal for quick discharge of capacitor resulting in reduction of pulse pile up. But, the level of thermal current noise in the input node is increased by low resistance values. The power spectral density of the feedback resistor current noise i2nR is inversely proportional to the resistance value R1 as shown in equation.

$$i_{nR}^2 = \frac{4kT}{R_1}$$

Where k is the Boltzmann constant and T is the absolute temperature. It is clear from equation (3.4) that R1 should be maintained at a very high ($\sim G\Omega$) to ensure noise reduction. However, maintaining the high value for R1 for long durations increases the chances of pulse pile up. The above two conflicting requirements have been met in the present design by utilizing a special reset scheme.

III. PLANAR SEMICONDUCTOR NEUTRON DETECTORS: DESIGN SIMULATIONS

This section discusses in detail, the simulations for optimization of thickness of converter layer for planar semiconductor neutron detectors. As noted in chapter 1, the efficiency of the detectors strongly depends on the type of converter material and relative dimensions of the converter vis-a-vis the semiconductor regions. The simulations have been carried out based on the method outlined by Shultis and Mc Gregor. As the dead layer also contributes to significant reduction in efficiency, the detailed simulation

pertaining to inclusion of dead layer is also discussed. The converter thickness is optimized by Monte Carlo technique implemented in MATLAB program. The planar configuration of the detector is built by geometrical modifications in trench structured neutron detectors. The effect of dead layers on efficiency is simulated by modification of this planar configuration by inclusion of the metal electrodes. The following sections discuss the factors affecting neutron detector design and their optimization / study through the above two simulations in detail.

IV. DESIGN EVOLUTION OF NEUTRON DETECTORS

Different designs for semiconductor neutron detectors have been explored and investigated in recent years. An important motivating factor for these efforts is the pursuit of high intrinsic neutron detection efficiency. The intrinsic neutron detection efficiency ($\boldsymbol{\epsilon_{int}}$), is defined as the probability that a neutron entering a detection volume gets registered in the detection system. In most applications, neutron detectors are operated in the pulse mode. In this mode of operation, the detector signal is a series of randomly spaced current pulses in time, each caused by the ions of a neutron capture. The time of occurrence of each pulse and its amplitude correspond to the time of arrival of the ions into the semiconductor region and their instantaneous energy, respectively. This raw detector signal is integrated in a charge sensitive preamplifier to generate a voltage pulse signal. The height of this voltage pulse represents the total energy deposited in the detection volume. Thus, for a neutron detector operating in the pulse mode, the $\boldsymbol{\epsilon_{int}}$, is defined as

$$\epsilon_{int} = \frac{\textbf{Number of pulses recorded}}{\textbf{Number of Neutrons incident on the detector}}$$

An important factor that affects the value of $\boldsymbol{\epsilon_{int}}$, is the probability of neutron capture. Not all the neutrons that enter the detection volume undergo capture interaction. The type of the Converter Material (CM) and its length along the path of the neutron beam determine the number of neutrons that undergo capture interaction. It is quantitatively described by the neutron beam attenuation equation (4.2) for a parallel beam of neutrons incident with a fluence Io on a CM.

$$I = I_o e^{-\Sigma capture^t}$$

Thus, the fluence I of the neutron beam exiting the CM with a macroscopic capture cross section $\Sigma capture$ decreases exponentially with an increase in the thickness t of the CM. For any finite thickness t, there are always some neutrons in the beam exiting the CM without undergoing capture.

Another major factor that affects the value of $\boldsymbol{\epsilon_{int}}$ is the energy straggling of ions. The energy straggling occurs due to a path-length distribution of the ions in CM, arising from the probabilistic nature of the depth at which the neutron capture occurs. Therefore, the actual kinetic energies deposited by the ions, in the semiconductor region range from near zero values to that with which they are emitted in the capture reaction. Extraneous phenomena like gamma emissions accompanying neutrons and electronic noise also cause pulses similar to those arising out of neutron interactions. But typically, these are low energy events and hence, their maximum pulse heights are limited to voltage levels, which are lower compared to the maximum pulse heights of neutron events. Moreover, due to the energy straggling effect, the probability of ion energies getting reduced to levels comparable to that of the extraneous events increases. In the operation of practical neutron detectors, the extraneous events are prevented from getting spuriously registered as neutron events by setting a minimum energy threshold known as the Low-level discrimination (LLD) energy. Only those voltage pulses with heights above a minimum voltage corresponding to the LLD energy, are considered as true neutron events and are registered. The energy straggling effect in conjunction with a higher LLD setting, increases the probability of rejecting true neutron events, thereby reducing $\boldsymbol{\epsilon_{int}}$. Based on these two important factors namely, the neutron-capture probability and the energy straggling effects in CM, $\boldsymbol{\epsilon_{int}}$ is defined more appropriately as.

$$\epsilon_{int} = \frac{N_{capture}}{N_{incident}} \times \frac{N_{above} LLD}{N_{capture}}$$

where Nincident is the total number of neutrons entering the detector volume, Ncaptureis the number of neutrons undergoing capture interaction, Nabove LLD is the number of ions entering the semiconductor region and depositing energy above the LLD. The first and the second ratios in the equation (4.3) are identified as

- The probability of the ions entering and depositing energy in the semiconductor region above the LLD.
- The probability of a neutron entering the detection volume undergoing capture

The emergence of various detector designs is attributed to the efforts in independently increasing the two probabilities mentioned above.

$\bar{E}^i_m(X)$ and $\bar{E}^i_m(E)$ ESTIMATION IN GOLD DEAD LAYER MEDIUM

The empirical relations $\bar{E}^i_m(X)$ and $\bar{E}^i_m(E)$ have been generated for the configuration. The converter materials considered in the simulation are B10and Li6F. Hence, the ion residual energy data are generated for the following ions and target conditions.

- The Lithium Li6 conversion reaction ions in gold (Au) medium.
- The Boron B10 conversion reaction ions in gold (Au) medium.

the B10neutron capture reaction has four possible ions, while the Li6 reaction produces a triton and an alpha particle. For the purpose of simulation, the ions of the former reaction are identified based on their initial energy as Alpha-1 (1.7762 MeV), Alpha-2 (1.4721 MeV), Lithium-1 (1.0133 MeV) and Lithium-2 (0.8398 MeV).

Empirical fits for B10and Li6 conversion ions in gold (Au) medium

Figures 8 and 9 show the transport data of B10ions in gold layer calculated using TRIM and SRIM. As outlined in section 4.4.4, the empirical fits were obtained for $\bar{E}^i_m(X)$ and $\bar{E}^i_m(E)$. The behavior of monotonic decrease of residual energy E with pathlength

Xis similar to that observed in the case of transport of ions in silicon and B10 converters. Tables 4-2 and 4-3 show the empirical fits obtained using Table Curve® for $\bar{E}_m^i(X) and\ \bar{E}_m^i(E)$ of each ion.

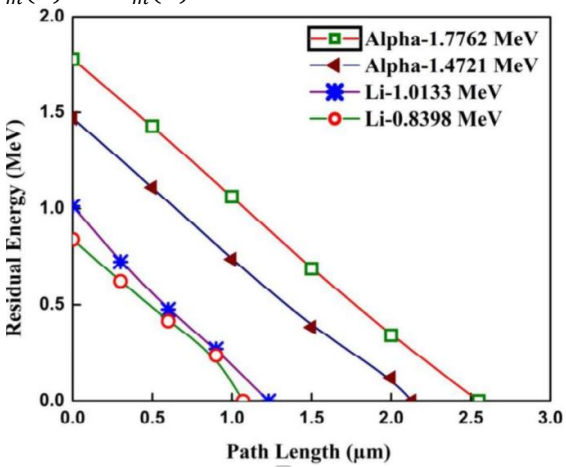

Fig. 8: Interpolated residual energy versus path length data for transport of Boron (B-10) neutron conversion ions in Gold (Au)

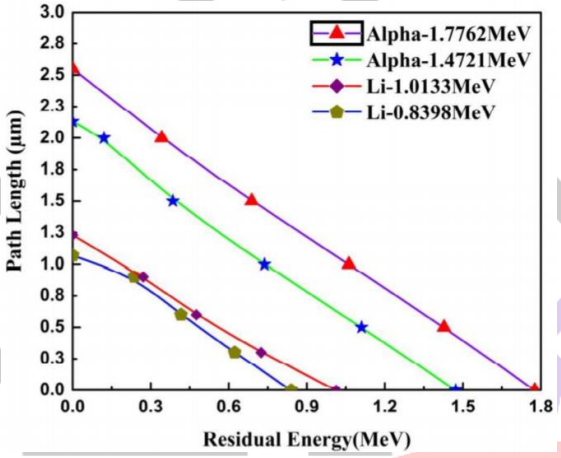

Fig. 9: Interpolated path length versus residual energy data for transport of Boron (B-10) neutron conversion ions in Gold (Au)

The Li6 neutron conversion reaction produces a triton and alpha particles which are emitted in the opposite directions with 2.73MeV and 2.05MeV, respectively. Figures 10 and 11 show the $\bar{E}_m^i(X) and\ \bar{E}_m^i(E)$ for these ions. Their empirical relations.

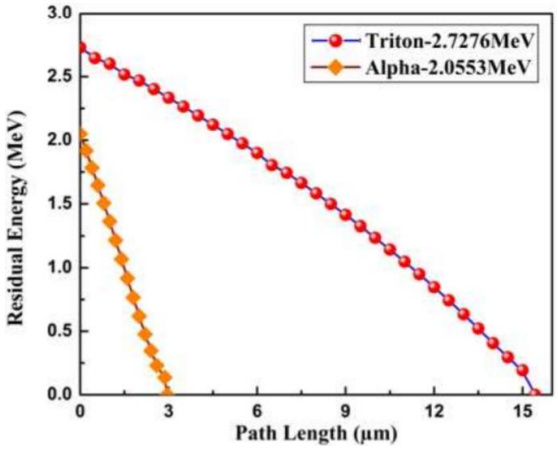

Figure 10: Interpolated residual energy versus path length data for transport of Lithium-6 neutron conversion ions in Gold (Au)

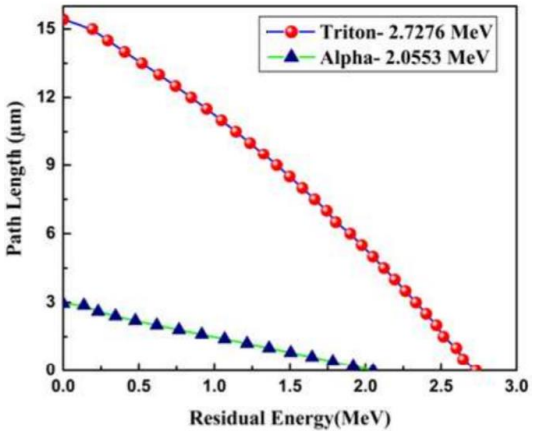

Figure 11: Interpolated path length versus residual energy data for transport of Lithum-6 neutron conversion ions in Gold (Au)

Detector Efficiency Simulation

Figure 12 shows the simulation of ϵ_{int} of a detector coated with B10and Li6Fconverter materials with varying gold dead layer thickness. The dead layer thickness is varied from 0.1 µm to 1.1 µm to emulate that encountered in practical devices. The efficiency decreases with increasing thickness. The LLD energy for this simulation was kept at 300 keV. From Figure 12 it can be observed that the ϵ_{int} of a Si diodegenerally decreases as the thickness of a sandwiched gold dead layer is increased. This is explained in terms of the effect of further reduction in the initial kinetic energy of the conversion reaction ions before they enter the depleted silicon region. In the model without the inclusion of the dead layer, most of the neutron conversion ions have their initial kinetic energy at or slightly above the LLD energy level. With the inclusion of dead layer, the events generating these are now prevented from getting registered as true neutron events because of the lower energy deposition. In this simulation, the thickness of the converter material was chosen to be the optimized value at tc, from a dead layer-sans detector as discussed in section 4.6. Hence, the thicknesses of the B10and Li6Fconverter materials are 2.5 and 25 µm, respectively. It is seen that the variation in efficiency with respect to the thickness of the dead layer follows different trends. For dead layer thicknesses less than 0.4 µm, the efficiency of a B10 coated diode is higher than that observed in the Li6Fcounterpart.For dead layer thickness higher than 0.6 µm, a B10 coated diode has a lower efficiency than a Li6F coated one. For the thicknesses of the dead layer between 0.4 µm to 0.6 µm, there is a steep decrease in efficiency from 3.9 % to 3.1% in the B10 coated diode, whereas the efficiency remains approximately constant at a value of 3.5% for a Li6Fcoated one in this range of thickness. In both the cases, the efficiency reduces to ~3% at a dead layer thickness of 1 µm.

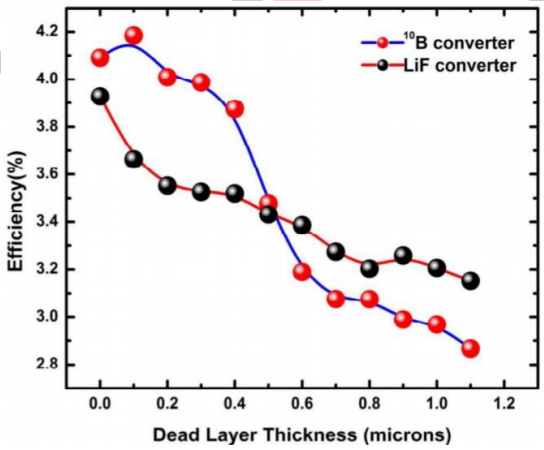

Fig. 12: Variation of the intrinsic neutron detection efficiency as the thickness of the dead layer is varied

Efficiency variation for both Boron and Li6F converter materials are shown. The higher efficiencies observed in the case of the B 10coated diodes as compared to the Li6Fcoated ones for low values of dead layer thickness below 0.4mm is due to the higher neutron absorption cross section for B10 (3840 barns), which is almost four times higher than that of Li6F (940 barns). From Figure 4.15, it is observed that there are two paths in the B10 neutron capture, viz., a reaction resulting in alpha-1 (1.7762 MeV) andlithium-1 (1.0133 MeV) with 6% branching ratio and another reaction resulting in alpha-2 (1.4721 MeV) and lithium-2 (0.8398 MeV) with 94% branching ratio. In the case of Li6F, the ions are triton (2.7276 MeV) and alpha (2.0553 MeV). The penetration depths of alpha-1, alpha-2 and the Li6F conversion alpha in gold layer are 2.55 µm, 2.13µm and2.95µm, respectively. The lithium ions from B 10 neutron capture (lithium-1 and lithium-2), being heavier than the triton (15.42 µm penetration depth) lose larger percentage of their energy (~80 %) and come to rest at 1.23 µm and 1.07 µm, respectively. Therefore, the combined effect of alpha and lithium

ions contribute to the ϵ_{int} of boron coated diodes upto 1 µm. Beyond 1 µm, the contribution is from the alpha particle alone. This is the reason for the low ϵ_{int} value in Boron coated diodes. Triton being lighter in mass as compared to lithium loses lesser energy (~5%) as it traverses gold for comparable thickness and therefore contributes significantly to the ϵ_{int} for thicknesses larger than 0.6 µm. The changeover from Boron to Lithium in ϵ_{int} is essentially a depiction of the energy deposited by the ions up to a maximum depth of ~ 2.95 µm.

V. CONCLUSION

In the present work, novel embedded readout electronics for existing portable radiation instruments have been designed and implemented. The cost effective and reliable designs were made possible by the use of recent advanced mixed signal programmable system on chip platform. A design optimization study of low-cost planar neutron detector has also been carried out. Brief conclusions of each of these studies are given below:

- A compact, reliable readout for Geiger Mueller detector was designed and implemented using the PSoC platform. The novel feature has been built in the design in which all the peripheral functions in a GM survey meter like, high voltage bias regulation and data communication along with the core counting function are integrated on to a single chip. The single chip implementation improves reliability by increased immunity to external interference and by providing mechanical ruggedness through miniaturization.
- The potential of recent reconfigurable mixed signal hardware platforms to implement cost effective and reliable readout electronics for portable radiation measurement applications is established after a thorough survey of different platforms and their functional capabilities. The importance of low-cost alternatives in detectors for achieving cost effective designs is also established.
- Design optimization studies of low-cost semiconductor neutron detectors in planar configuration have been carried out using Monte Carlo simulations. Preliminary work is done in optimizing the neutron converter material thickness for maximum intrinsic neutron detection efficiency for a planar neutron detector. Additional simulation of the effects of dead layer inclusion on the efficiency is performed by suitable modifications in the existing Monte Carlo model thus establishing the effects of dead layer in a practical device.
- Novel embedded pulsed reset technique-based readout electronics for an alpha spectrometer has been successfully designed and implemented. The pulsed reset technique controls the functioning of the feedback network of the preamplifier stage using a solid-state analog switch. In addition to this the spectrometer also features novel designs like ramped high voltage supply for detector biasing and data communication to PC based graphical user interface. Again, the single chip implementation of these features improves the reliability of the portable spectrometry application at an affordable cost.

In general, the count rate of pulses from GM tube, when exposed to gamma photons, is affected by both the actual exposure rate as well as the gamma energy. This is because the intrinsic detection efficiency of a GM tube itself is different at different gamma energies. In the present work on GM counter embedded readout the design is suitable for measuring accurate dose rates only with an energy compensated GM tube. An energy compensated GM tube is covered with a thin layer of metals such as lead and/or tin. This metal covering is done so as to empirically match the efficiency versus energy curve to the exposure per gamma photon versus energy for a given tube. This augmentation is made possible once the survey meter sensitivity versus energy data is available and can be incorporated as a look up table in the firmware. The correction factors from this look up table can be included in the engineering conversion codes of the firmware. Additional features like battery monitoring and test can be included.

The neutron detector optimization simulations can be further improved by incorporating composite dead layers in the unit cell. Further advanced semiconductor detector alternatives like neutron converter coated avalanche photodiodes with statistically varying multiplication factors can be substituted in place of simple PIN diode-based structures in the Monte Carlo simulations for efficiency calculations. The alpha spectrometer application can be further improved by incorporating features such as isotope identification, user controlled ramping rate, long term stability monitoring and battery monitoring in the firmware. Further modifications in the reset switch control waveform and the use of recent advanced ultra-low charge injection switches can be incorporated in the hardware to reduce the residual errors in pulse height measurement thereby enhancing the resolution.

REFERENCES

[1] Luís Marques, Alberto Vale and Pedro Vaz (2021) State-of-the-Art Mobile Radiation Detection Systems for Different Scenarios Sensors 2021, 21, 1051. https://doi.org/10.3390/ s21041051

[2] G. Prasanna and J. Jayapandian (2014) An embedded read-out for GM counter Int. J. Instrumentation Technology, Vol. 1, No. 3, 2014

[3] B. S. Buddena, L. C. Stonehilla, A. Warnimenta, J. Michela, S. Stormsa, N. Dallmanna, D. D. S. Couplanda, P. Steina, S. Wellera, L. Borgesa, M. Proicoua, G. Durana, J. Kamto (2015) Handheld Readout Electronics to Fully Exploit the Particle Discrimination Capabilities of Elpasolite Scintillators Nuclear Instruments and Methods in Physics Research Section A Accelerators Spectrometers Detectors and Associated Equipment 795. https://www.researchgate.net/publication/279245868_Handheld_readout_electronics_to_fully_exploit_the_particle_discrimination_capabilities_of_elpasolite_scintillators

[4] G. P. Srivastava (2013) Electronics in nuclear power programme of India—An overview Sadhan ¯ a¯ Vol. 38, Part 5, October 2013, pp. 897–924. c Indian Academy of Sciences

[5] Wolfgang Hennig and Shawn Hoover (2020) White Rabbit Time Synchronization for Radiation Detector Readout Electronics https://arxiv.org/abs/2010.15259

[6] B. D. Milbrath, A. J. Peurrung, M. Bliss and W. J. Weber (2008) Radiation detector materials: An overview Journal of Materials Research , Volume 23 , Issue 10 , October 2008 , pp. 2561 – 2581. DOI: https://doi.org/10.1557/JMR.2008.0319

[7] Pradeep Kumar, K.A.; Shanmugha Sundaram, G.A.; Sharma, B.K.; Venkatesh, S.; Thiruvengadathan, R. Advances in gamma radiation detection systems for Emergency Radiation Monitoring. Nucl. Eng. Technol. 2020, 52, 2151–2161.

[8] Watkins, S.; Burry, J.; Mohamed, A.; Marino, M.; Prudden, S.; Fisher, A.; Kloet, N.; Jakobi, T.; Clothier, R. Ten questions concerning the use of drones in urban environments. Build. Environ. 2020, 167, 106458.
[9] Ihantola, S.; Tengblad, O.; Chitumbo, N.; Csome, C.; Eisheh, J.-T.; Kröger, E.; Paepen, J.; Peräjärvi, K.; Röning, J.; Schneider, F.; et al. Impact of Novel Technologies on Nuclear Security and Emergency Preparedness: ERNCIP Thematic Group Radiological & Nuclear Threats to Critical Infrastructure; Publications Office of the European Union: Luxembourg, 2019; ISBN 978-92-76-09668-9.
[10] P. Riley, A. Enqvist, S.J. Koppal, Low-cost depth and radiological sensor fusion to detect moving sources, in: 2015 International Conference on 3D Vision, 2015, pp. 198e205.
[11] J.M. Nilsson, K. Ostlund, J. S € oderberg, S. Mattsson, C. R € € aaf, Tests of HPGe- and € scintillation-based backpack g-radiation survey systems, J. Environ. Radioact. 135 (2014) 54e62.
[12] B. Sanaei, M.T. Baei, S.Z. Sayyed-Alangi, Characterization of a new silicon photomultiplier in comparison with a conventional photomultiplier tube, J. Mod. Phys. 6 (2015) 425e433.
[13] H.M. Park, K.S. Joo, Remote radiation sensing module based on a silicon photomultiplier for industrial applications Appl, Radiat. Isot. 115 (2016) 13e17.
[14] H. Yoo, S. Joo, S. Yang, G. Cho, Optimal design of a CsI (Tl) crystal in a SiPM based compact radiation sensor, Radiat. Meas. 82 (2015) 102e107.
[15] M. Grodzicka, M. Moszynski, T. Szcze ˛sniak, M. Kapusta, M. Szawłowski, D. Wolski, Energy Resolution of Small Scintillation Detectors with SiPM Light Readout JINST 8, 2013, pp. 2017e2034.
[16] G.F. Knoll, Radiation Detection and Measurement, fourth ed., John & Wiley Sons Inc, 2010, pp. 241e242.